

Electronic Supplementary Information

Probing surface-sensitive redox properties of VO_x/TiO₂ catalyst nanoparticles

Martin Ek^{a,b}, Logi Arnarson^a, Poul Georg Moses^a, Søren B. Rasmussen^a, Magnus Skoglundh^c, Eva Olsson^b, and Stig Helveg^{*a,d}

^a Haldor Topsoe A/S, Haldor Topsøes Allé 1, DK-2800 Kgs. Lyngby, Denmark

^b Competence Centre for Catalysis, and Department of Physics, Chalmers University of Technology, 41296 Göteborg, Sweden

^c Competence Centre for Catalysis, and Department of Chemistry and Chemical Engineering, Chalmers University of Technology, 41296 Göteborg, Sweden

^d Center for Visualizing Catalytic Processes (VISION), Department of Physics, Technical University of Denmark, DK-2800 Kgs. Lyngby, Denmark

*E-mail: stig@fysik.dtu.dk

Supplementary Figures

S1. Illustration of STEM-EELS acquisition method.

S2. Reference EEL spectra of vanadium oxides.

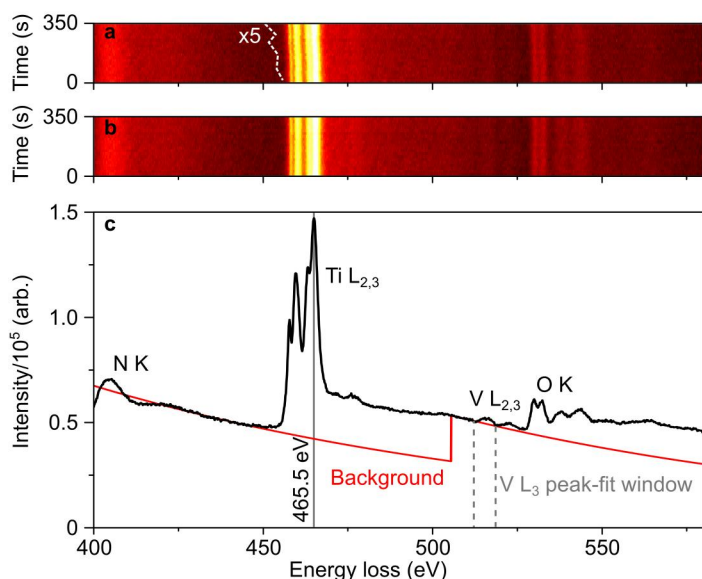
S3. Mitigation of beam-induced alterations.

S4. Reversibility of vanadium oxidation and reduction.

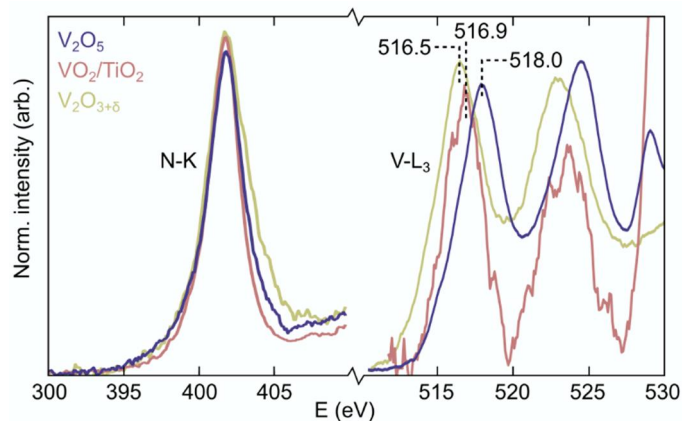
S5. Analysis of VO_x/TiO₂ nanoparticle morphology.

S6. Suppression of beam-induced alterations in STEM-EELS acquisition.

Supplementary references



Supplementary Figure S1. Illustration of STEM-EELS acquisition method. (a) EEL spectrum image (SI) containing 80 four second exposures (in this case recorded as 20 separate spectra each averaging four exposures). After adding each new spectrum to the SI, the drift-tube voltage was stepped 0.3 V to shift the spectrum over the CCD. After compensating for the intentional shift, the remaining unintentional drift and instabilities are visible particularly in the strong Ti-L edge from the fact that consecutive spectra do not line up perfectly (exaggerated 5 times by the dashed line). (b) The same SI after aligning the individual spectra to the Ti-L edge. (c) The spectrum produced by summing the SI from **b**. A power-law background was fitted prior to the Ti and V-L edges and extrapolated as indicated, after which the energy loss scale was adjusted to place the peak of the Ti-L₂ feature at 465.5 eV. The Ti signal stems mainly from the interior of the anatase nanoparticles and is insensitive to changes in the environment, which makes it an ideal energy reference. The N-K edge, just visible at the start of the EEL spectrum, stems from the supporting Si₃N₄ film of the MEMS device. The 7 eV window used for fitting the V-L₃ feature is also indicated in **c**, centred on the peak position, showing the limits imposed by the nearby V-L₂ at higher energies. At lower energies, the limit ultimately stems from the change in background slope at around 500 eV. However, in practice there is no point in including energy losses below about 510 eV, as this region contains no signal from the V-L₃ feature.



Supplementary Figure S2. Reference EEL spectra of vanadium oxides. EEL spectra acquired from bulk V_2O_5 , anatase-supported vanadium oxide reduced in H_2 (VO_2/TiO_2), and bulk V_2O_3 . The V-L₃ energy losses measured from these samples comprise the basis for the vanadium oxidation state reference values used throughout the main text. The sharp nitrogen K-edge from added N_2 (1 mbar) is used as an internal reference for aligning the spectra to the same energy loss scale. For VO_2/TiO_2 , this procedure is conducted in two steps by first aligning the N-K (401.8 eV) and Ti-L₂ (465.5 eV) energy losses, and subsequently aligning the Ti-L₂ and V-L₃ energy losses during H_2 reduction.

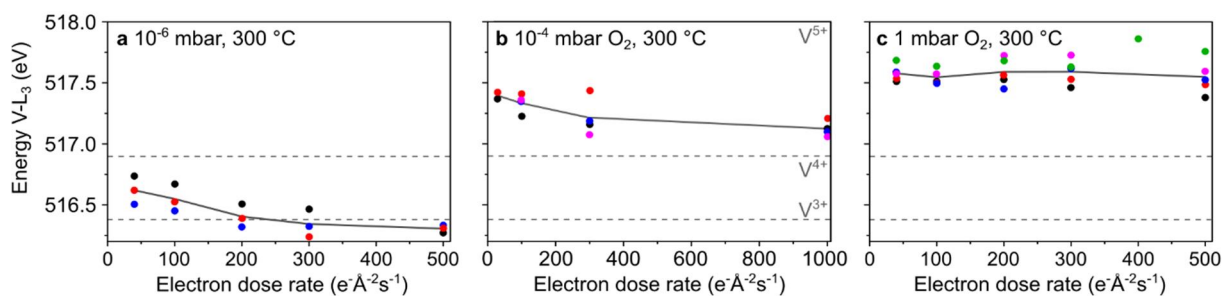
For V_2O_5 , the V-L₃ energy loss measured in 1 mbar O_2 is 518.0 eV (measured at room temperature using a conventional double-tilt specimen holder). The measured energy loss is furthermore consistent with the 517.94 eV energy loss measured for VO_x/TiO_2 under the most oxidizing conditions ($O_2:NO$ 1 mbar: 0.1 mbar). Consequently, the V^{5+} reference value is set to 518.0 eV.

For V_2O_3 , there is a risk of oxidation during sample preparation in air. The sample is therefore heated *in situ* to 600 °C using a furnace-type specimen holder (Gatan 628 inconel) in N_2 during the measurement,¹ yielding a V-L₃ energy loss of 516.5 eV. There are however reasons to suspect that the sample nonetheless is slightly oxidized to $V_2O_{3+\delta}$: both the vanadium V-L₃/L₂ intensity ratio and the V-L₃ energy loss shift compared to V_2O_5 are smaller than previously reported for V_2O_3 .¹ A V^{3+} reference value of 516.4 eV is therefore chosen as it (1) aligns with previously reported EELS¹ and XPS² results, (2) is consistent with the lower bound found for VO_x/TiO_2 catalysts under reducing conditions, and (3) is close to the value measured for $V_2O_{3+\delta}$.

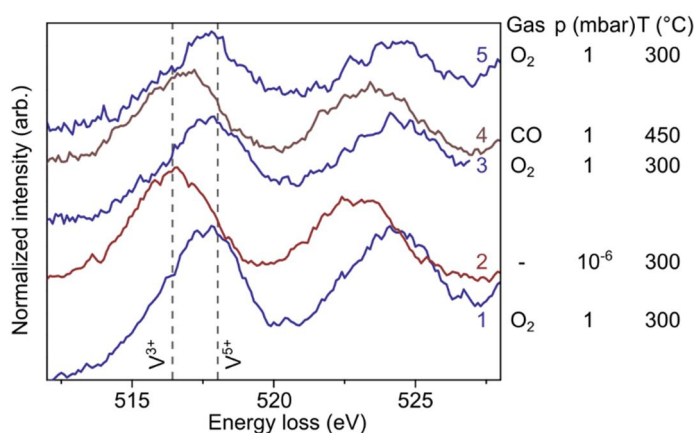
For the V^{4+} reference, *in situ* reduction of VO_x/TiO_2 by H_2 (1 mbar, heated to 300 °C using a Protochips MEMS device) is used³ – a procedure shown to yield the V^{4+} oxidation state in an XPS study by Kim et al.⁴ The V^{4+} reference value thus measured is 516.9 eV, giving an energy loss shift from V^{5+} that is consistent with XPS studies,² but larger than reported by EELS.¹ The

alternative use of bulk V_2O_4 for the V^{4+} reference would come with uncertainties regarding both oxidation during sample preparation and reduction in the microscope vacuum.

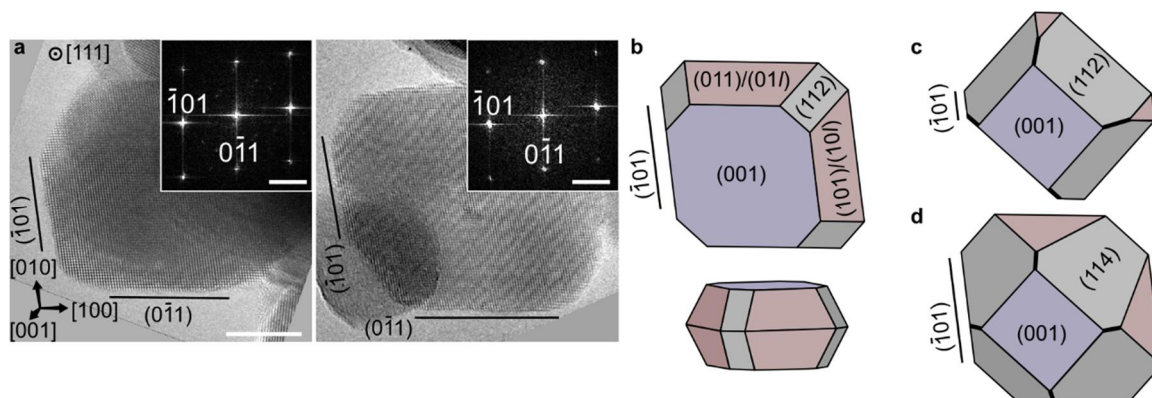
Overall, the reference measurements show a consistent decrease in V-L₃ energy loss when reducing vanadium oxides. The consistency over multiple sample types and with previous reports means that the V^{5+} reference value can be considered well established, while there are some uncertainties regarding the exact value for V^{3+} and in particular V^{4+} . However, the main point of this report – the existence of differences in oxidation states between facets – is insensitive to adjustment of these values.



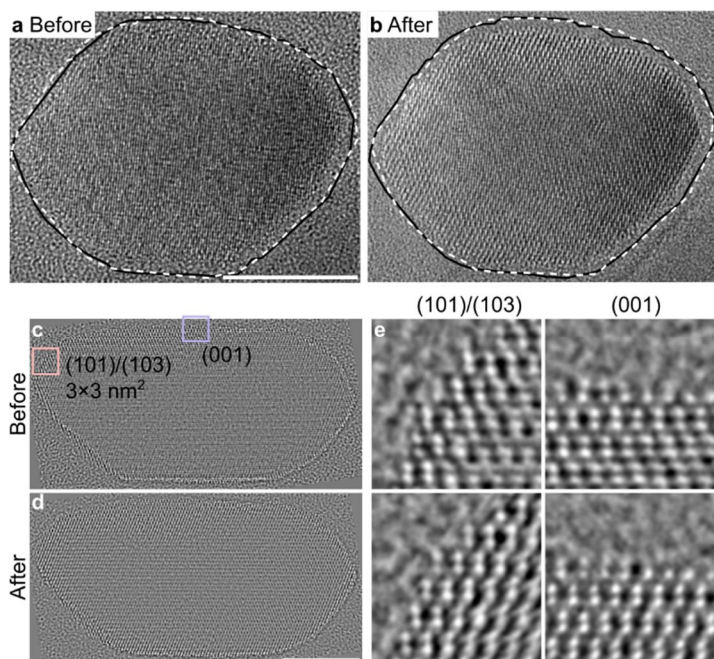
Supplementary Figure S3. Mitigation of beam-induced alterations. The beam-induced reduction of VO_x on TiO₂, is examined by EELS, using the shift of the V-L₃ energy loss, as a function of the electron dose rate under various environmental conditions. We have previously determined that beam-induced reduction is determined primarily by the electron dose rate, with no detectable influence from the total accumulated dose.³ For each dose rate, EEL spectra are collected for a few different agglomerates, each represented by a set of coloured point in the graphs. **(a)** In vacuum (10⁻⁶ mbar), a slight shift to lower V-L₃ energy losses occurs already above 100 e⁻Å⁻²s⁻¹. Above 200 e⁻Å⁻²s⁻¹, the shift indicates that a reduction further than VO_{1.5} occurs. **(b)** In a 10⁻⁴ mbar O₂ atmosphere at 300 °C, beam-induced reduction becomes noticeable at electron dose rates higher than ca. 200-300 e⁻Å⁻²s⁻¹, with the exact onset varying from agglomerate to agglomerate. Even at high dose rates of 1000 e⁻Å⁻²s⁻¹, the shift amounts to no more than 0.3 eV. **(c)** At a higher O₂ pressure of 1 mbar, no overall trend is seen over the investigated electron dose rate interval, although a few individual agglomerates still show small shifts in the V-L₃ to lower energy losses.



Supplementary Figure S4. Reversibility of vanadium oxidation and reduction. Vanadium L-edge region from EEL spectra recorded from agglomerates of VO_x/TiO₂ particles during the oxidation/reduction cycle illustrated in Figure 2 in the main text. The spectra were recorded in order from 1 to 5. The signal has in each case been normalized to the Ti-L₂ intensity and has only been offset vertically to allow easier comparison. The similar intensities are therefore an indication of an even distribution of vanadium oxides over the TiO₂ particles. The small variations in the intensities that nonetheless do appear can be attributed to either correspondingly small variations in vanadium coverage or average TiO₂ particle sizes, affecting the average surface to volume ratio, between the agglomerates. The shift in the V-L₃ energy loss between oxidizing and reducing conditions is fully reversible and comparable to that measured between bulk V₂O₅ and V₂O₃.



Supplementary Figure S5. Analysis of VO_x/TiO_2 nanoparticle morphology. (a) TEM images of VO_x/TiO_2 nanoparticles viewed in $[111]$. In this projection the $\{101\}$ facets form a parallelogram outline with truncated corners which indicate the presence of additional $\{11l\}$ facets with $l > 1$. Scale bar, 10 nm. Inset FFTs are shown to support the indexing. Scale bar, 2 nm^{-1} . (b) Proposed shape of the particle with $l = 2$, that matches the outlines in **a** together with a smaller 3D model. (c) For very large $\{11l\}$ facets, an edge is formed (marked with a thicker line) which, if viewed in $[010]$, might be mistaken for a $\{10l\}$ type high-index facet. However, for $l = 2$ the resulting shape is not consistent with the particles in **a**. (d) Choosing instead e.g. $l = 4$ provides a better match to the particles, but the edges are now only formed at the parts closest to the $\{001\}$ facet. The outline of the particles when viewed in $[111]$ therefore provides strong evidence that the $\{10l\}$ facets discussed in the main text are “true” facets, and not just an edge between two facets not parallel to the $[010]$ viewing direction. In particular, the area shown in Figure 3 in the main text is very close to the $\{101\}$ facet and therefore very unlikely to correspond to an edge rather than the proposed $\{102\}$.



Supplementary Figure S6. Suppression of beam-induced alterations in STEM-EELS acquisition. HRTEM images recorded under oxidizing conditions (a) before and (b) after recording EEL spectra in STEM mode as shown in Figure 2 a-c in the main text. The contrast changed slightly between the two images due to a small change in the orientation of the particle. However, tracing the outline of the particle (enlarged 6% in the images so as not to obscure the particles themselves) reveals that no large scale changes in the particle structure or morphology occurred from the exposure to the focused electron beam used in STEM mode. Scale bar, 10 nm. (c) Exit wave phase image reconstructed from a focal series recorded under oxidizing conditions *prior* to performing STEM-EELS measurements. (d) Exit wave phase image of the same particle, recorded *after* performing the STEM-EELS measurements included in Figure 3 in the main text. Scale bar, 10 nm. (e) Cropped details from two different facet types, marked in c, to further illustrate the absence of changes at the atomic level. The use of exit wave reconstructions enables high sensitivity at low electron dose rates⁵ and facilitates structural interpretation.⁶ The exit wave reconstructions are based on series of 35 high-resolution TEM images acquired with 3 s exposure times and 2 nm defocus steps ($C_1 = 40$ to -30 nm). Reconstructions were performed using the Gerchberg-Saxton algorithm⁷ as implemented in the MacTempas software (www.totalresolution.com).

Supplementary references

- 1 D. S. Su, M. Wieske, E. Beckmann, A. Blume, G. Mestl and R. Schlögl, *Catal. Letters*, 2001, **75**, 81–86.
- 2 E. Hryha, E. Rutqvist and L. Nyborg, *Surf. Interface Anal.*, 2012, **44**, 1022–1025.
- 3 M. Ek, Q. M. Ramasse, L. Arnarson, P. G. Moses and S. Helveg, *Nat. Commun.*, 2017, **8**, 305.
- 4 C. Y. Kim, J. W. Elam, P. C. Stair and M. J. Bedzyk, *J. Phys. Chem. C*, 2010, **114**, 19723–19726.
- 5 S. Helveg, C. F. Kisielowski, J. R. Jinschek, P. Specht, G. Yuan, H. Frei, *Micron*, 2014, **68**, 176–185.
- 6 S. Van Aert, P. Geuens, D. Van Dyck, C. Kisielowski, J. R. Jinschek, *Ultramicroscopy*, 2007, **107**, 551–558.
- 7 R. W. Gerchberg, W. O. Saxton, *Optik*, 1972, **35**, 237–246.